TISSUE ENGINEERING: Part C
Volume 21, Number 2, 2015

DOI: 10.1089/ten.tec.2014.0110

Viability, Differentiation Capacity, and Detectability of Super-Paramagnetic Iron Oxide-Labeled Muscle Precursor Cells for Magnetic-Resonance Imaging

Fahd Azzabi, PhD,[1] Markus Rottmar, PhD,[1,2] Virginija Jovaisaite, MSc,[1] Markus Rudin, PhD,[3] Tullio Sulser, MD,[1] Andreas Boss, MD, PhD,[2] and Daniel Eberli, MD, PhD[1]

Cell therapies are a promising approach for the treatment of a variety of human conditions including stress urinary incontinence, but their success greatly depends on the biodistribution, migration, survival, and differentiation of the transplanted cells. Noninvasive *in vivo* cell tracking therefore presents an important aspect for translation of such a procedure into the clinics. Upon labeling with superparamagnetic iron oxide (SPIO) nanoparticles, cells can be tracked by magnetic resonance imaging (MRI), but possible adverse effect of the labeling have to be considered when labeling stem cells with SPIOs. In this study, human muscle precursor cells (hMPC) were labeled with increasing concentrations of SPIO nanoparticles (100–1600 μg/mL) and cell viability and differentiation capacity upon labeling was assessed *in vitro.* While a linear dependence between cell viability and nanoparticle concentration could be observed, differentiation capacity was not affected by the presence of SPIOs. Using a nude mouse model, a concentration (400 μg/mL) could be defined that allows reliable detection of hMPCs by MRI but does not influence myogenic *in vivo* differentiation to mature and functional muscle tissue. This suggests that such an approach can be safely used in a clinical setting to track muscle regeneration in patients undergoing cell therapy without negative effects on the functionality of the bioengineered muscle.

Introduction

Stress urinary incontinence (SUI)–the involuntary loss of urine–is a medical problem affecting millions of people worldwide.[1] While this condition not only markedly decreases the quality of life of patients, annual direct costs of caring amounts to $16 billion in the United States alone.[2] SUI occurs mainly due to a malfunction of the sphincter muscle, which is located around the urethra and prevents urine from leaking out of the bladder. If damaged, different strategies including physical exercise, medications, interventional therapies or surgery are currently used to treat the patient. However, such procedures alleviate the symptoms only temporarily without providing permanent or at least long-term solutions.[3–5]

Stem cell therapies are a promising approach for the treatment of human conditions where currently only limited or no treatment options are available. Envisioned to replace damaged or diseased cells, tissues, or organs in patients, a range of stem cell therapy concepts that target different pathologies including conditions of the heart, muscular dystrophy, diabetes, or Parkinson's disease are currently being developed.[6–11]

Recent research shows that similar strategies using stem cells have the potential to restore normal sphincter function in patients affected by SUI.[12,13] Stem cells can be either of embryonic or adult origin and can be further divided in muscular or nonmuscular cell types, which include but are not limited to muscle precursor cells (MPCs), satellite cells from muscle fibers, muscle-derived stem cells, mesenchymal stem cells (MSCs), hematopoietic stem cells, and adipose stem cells.[12] MPCs are a promising source due to their skeletal muscle origin and their restricted differentiation potential toward muscle, which has been supported by excellent results in a large animal model showing a restoration of 80% of initial sphincter pressure upon injection of MPCs in dogs.[14]

The success of cell therapy approaches greatly depends on the biodistribution, migration, survival, and differentiation of the transplanted cells. Tracking of the hMPCs after injection *in vivo* therefore presents an important aspect for translation of such a procedure to the clinics. While traditional histopathological techniques are too invasive to localize the injected cells in a clinical setting, cellular imaging approaches represent a noninvasive tool to follow implanted stem cells and to evaluate the success of the therapeutic treatment.[15,16] The most frequently employed techniques for cell tracking include magnetic resonance imaging (MRI), radioactive labeling for positron emission tomography and single photon emission computed tomography, bioluminescence, and

[1]Division of Urology and [2]Institute of Diagnostic and Interventional Radiology, University Hospital Zurich, Zurich, Switzerland.
[3]Institute for Biomedical Engineering, ETH and University of Zurich, Zurich, Switzerland.

fluorescence. For clinical application, MRI is considered a method of choice to track stem cells *in vivo* because of its high spatial resolution on soft tissue structures, therefore providing anatomical details of the graft area, which may also help in detecting inflammation or edema.[17,18] Moreover, MRI is a well-established technology available in most clinical centers.

While MRI offers excellent soft tissue contrast by design, application of contrast enhancing gadolinium-chelates has become an established tool in clinical practice. However, the altered signal intensities between different tissues upon application of intravenous contrast media mainly rely on differences in uptake and washout of the agent, and the relaxivity of the applied gadolinium complex. Specificity of a contrast agent is of paramount importance for identification and tracking of specific entities such as cells and tissues but the development of targeted, mostly peptide-based contrast agents is still in its infancy.[19] In the case of cell-based tissue engineering concepts, nanoparticles that interfere with the magnetic field can be used to label the cells prior to their use *in vivo*. Such magnetic nanoparticles can be composed of different elements including iron, manganese, or gadolinium but the most popular ones are the superparamagnetic iron oxide (SPIO) nanoparticles, which consist of an iron oxide core with a polymeric or polysaccharide coating such as dextran, carboxydextran, or polyethylene glycol to facilitate stabilization and solubility of the particles.[20] Provoking local field inhomogeneities and subsequent spin-dephasing, SPIO nanoparticles lead to a decreased signal on T2-weighted MR images, thereby enabling the detection of the labeled cells as a hypo-intense signal in the MR image.

Two SPIO formulations, ferumoxides (Feridex®/Endorem®) and ferucarbotran (Resovist®), are approved by the FDA for clinical use in liver imaging,[21] and have been used to label stem cell types from different origin, including neural, endothelial, mesenchymal, and hematopoietic tissues.[22–26] Assessing the possible negative effects of SPIO labeling on the stem cell phenotype and cell behavior, reports significantly differ and range from no effect to a minimal negative effect on cell viability to inhibition of differentiation and migration.[23–25,27–30] As not only labeling efficiency, but also cell survival and behavior appears cell and SPIO dependent, proliferation and differentiation analysis should be considered when labeling stem cells with SPIO.[31–34]

In this study, we demonstrate the labeling of hMPCs with SPIO nanoparticles without additional transfection agents and evaluate the possibility to track these cells over time in a noninvasive manner. We present data defining the optimal concentration for SPIO labeling without a negative effect on viability, differentiation, and myofiber formation. Furthermore, we show that SPIO-labeled muscle tissue remains traceable by T2-weighted MRI scans for 4 weeks and that labeled hMPCs form muscle tissue *in vivo* with contractile forces comparable to nonlabeled tissues, demonstrating that such an approach would be suitable to monitor muscle regeneration in a clinical setting.

Materials and Methods

Cell culture

hMPCs were derived from *rectus abdominis* muscle samples of consenting patients undergoing abdominal surgery at the UniversityHospital Zurich. This procedure was approved by the local ethics committee. The hMPCs were harvested following established protocols.[14,35] Briefly, muscle biopsies were minced and digested for 1 h at 37°C 5% CO_2 in DMEM/F-12 (Gibco, Invitrogen) with 0.2% collagenase type I (Worthington Biochemical) and 0.4% dispase (Gibco, Grand Island). Samples were centrifuged, filtrated, and plated on collagen-coated six-well dishes. To reduce the number of fast adhering fibroblasts, the MPC-containing suspension was replated after 24 h. Cells that attached to culture wells by day 4 after replating were used. hMPCs were cultured at 37°C in 5% CO_2 with growth medium containing DMEM/F-12 (Gibco, Invitrogen) supplemented with 18% fetal bovine serum (Gibco, Invitrogen), 1% penicillin/streptomycin (Gibco, Invitrogen), 10 μg/mL human epidermal growth factor (hEGF; Sigma), 1 μg/mL human basic fibroblast growth factor (hbFGF; Sigma), 10 μg/mL human insulin (Sigma), and 0.4 μg/mL dexamethasone (Sigma).

SPIO labeling

Cells were labeled with the clinically approved contrast agent Endorem (Guerbet AG), consisting of dextran-coated SPIO nanoparticles with a size distribution between 120 and 180 nm and an iron content of 11.2 mg/mL. hMPCs of the second passage were cultivated in growth medium supplemented with 100, 200, 400, 800, or 1600 μg/mL SPIO nanoparticles. After 24 h incubation the labeling medium was removed and cells were analyzed.

Prussian blue staining

The efficiency of SPIO labeling was determined by Prussian blue staining. Unlabeled (control) and labeled MPCs were washed with phosphate-buffered saline (PBS), fixed with 4% paraformaldehyde for 15 min, incubated for 30 min with 2% potassium ferrocyanide (Sigma) in 2% hydrochloric acid solution (Perl's reagent), and counterstained with nuclear fast red (Sigma).

Viability

Viability of SPIO-labeled MPCs was assessed by Trypan Blue (Sigma) exclusion assay 24 h after iron oxide addition. After trypsinizing, the blue positive (nonviable) and unstained (live) cells were counted separately; a minimum of 100 cells per condition per sample were counted in total.

Cell proliferation

Cell proliferation was evaluated by MTT assay for two passages after labeling. Labeled MPCs were seeded in 24-well plates at a density of 3000 cells/cm^2. To generate a growth curve, triplicates of each condition were analyzed by MTT assay every 24 h for 7 days. Cells were incubated with growth medium containing 0.5 mg/mL Thiazolyl blue (Sigma) for 1 h at 37°C. After removing the media, cells were lysed with dimethyl sulfoxide (Sigma) for 15 min and the intensity of the color was measured at 570 nm with a Synergy HT Microplate reader (BioTek Instruments, Inc.).

Myogenic differentiation

To induce myogenic differentiation, MPCs were cultured for 8 days in differentiation medium, containing DMEM/F-12

(Gibco, Invitrogen) supplemented with 10% fetal bovine serum (Gibco, Invitrogen) and 1% penicillin/streptomycin (Gibco, Invitrogen). The hMPCs treated with SPIO for 24 h were subjected to this regimen directly after the labeling and in the following passage.

To evaluate the myofiber formation cells were fixed with methanol for 7 min, air dried, and stained with Giemsa solution (diluted 1:20 with deionized water; J.T. Baker) for 1 h. Number of nuclei per fiber and percent of fused cells were counted in five pictures of 20× magnification taken for each SPIO labeling condition. A differentiation ratio was calculated by dividing the nuclei in fibers by all nuclei.

Flow cytometry analysis

Labeled MPCs at P2 were split and cultivated until confluence prior to flow cytometry analysis. Harvested MPCs were fixed in 2% formaldehyde for 10 min and permeabilized in 0.5% Triton X-100 for 7 min. Primary mouse antibodies raised against human IgG (1:40; Santa Cruz), MyoD (1:100; BD Pharmingen), myosin heavy chain (MyHC, 1:100; Santa Cruz), desmin (1:100; Sigma), α-actinin (1:200; Sigma), and CD34 (1:100; BD Biosciences) and secondary fluorescent goat anti-mouse IgG-FITC (1:200; BD Pharmingen) were used for analysis. Cell fluorescence was measured with a Becton-Dickinson FACS Canto Machine and data were analyzed using FlowJo software.

Immunofluorescence

After labeling MPCs were fixed in 4% paraformaldehyde for 10 min, permeabilized in 0.5% Triton X-100 for 7 min and blocked with 1% bovine serum albumin (BSA) for 20 min. Primary mouse antibodies raised against human MyoD (1:50; BD Pharmingen), MyHC (1:100; Santa Cruz), desmin (1:100; Sigma), α-actinin (1:500; Sigma), and secondary rabbit anti-mouse antibody Cy3 IgG (1:1000; Sigma) together with Phalloidin (1:100; Sigma) and DAPI (1:100; Sigma) were used for staining.

Cell transplantation

A total of 44 nude female mice (CD-1.nu-Crl1, Crl:CD1-Foxn1nn; Charles River Laboratories) were used as hMPC recipients. The mice were split into two groups with 22 mice each and each group received injections with either control cells or SPIO-labeled cells. All procedures were performed in accordance with the regulations of the cantonal veterinary office Zurich.

hMPCs were labeled with 400 μg/mL SPIO for 24 h before injection. Unlabeled hMPCs were used as a control. Cells were washed with PBS (Gibco, Invitrogen), labeled using a PKH67 green fluorescent dye (Sigma), and suspended in 1% collagen type I solution (BD Biosciences). Subcutaneous injections of 1×10^7 hMPCs were performed on the left and right sides of the back of nude mice. During injection animals were anesthetized with 3% isoflurane.

Histology

After sacrificing the mice, the tissue-engineered muscles were excised from the back, fixed in formalin for 48 h, embedded in paraffin, and sectioned at 5 μm. For Prussian blue staining, the sections were deparaffinized and stained in Perl's reagent (2% potassium ferrocyanide [Sigma] in 2% hydrochloric acid solution) for 20 min at 60°C. Slides were counterstained with nuclear fast red (Sigma).

For immunostaining, the sections were deparaffinized, permeabilized in 0.1% Proteinase K (Sigma) solution for 30 min at 37°C, and blocked with 5% BSA 0.3% Triton X-100 for 1 h. Primary mouse antibodies against human MyHC (1:100; Santa Cruz), desmin (1:50; Sigma), and α-actinin (1:500; Sigma) and secondary rabbit anti-mouse antibody Cy3 IgG (1:1000; Sigma) together with DAPI (1:100; Sigma) were used for muscle fiber staining.

Macrophage staining was performed on paraffinized sections using primary rat antibody against mouse F4/80 (1:100; BMA Biomedicals) and secondary biotinylated anti-rat IgG (1:200; Vector Laboratories) with ABC reagent. Liquid DAB + Substrate Chromogen System (Dako) was used to visualize the staining.

To visualize PKH67 staining, the tissue strips were frozen and sectioned at 15 μm. Sections were fixed with 4% formalin and autofluorescence was reduced by incubation with 0.3 M glycine (Sigma) in PBS. Sections were counterstained with DAPI (1:100; Sigma).

Organ bath

Two and 4 weeks after hMPC injection, the tissues were harvested and their contractility evaluated. The muscle strips were fastened with suture loops in Radnoti tissue bath chambers. The tissues were immersed in Krebs solution (119 mM NaCl, 4.4 mM KCl, 20 mM $NaHCO_3$, 1.2 mM NaH_2PO_4, 1.2 mM $MgCl_2$, 2.5 mM $CaCl_2$, and 11 mM glucose) under constant oxygenation at room temperature. Muscle strips were stimulated with increasing electrical-field stimulation (40 Hz at 40 V and 80 Hz at 80 V). Contractions were recorded and their values were normalized to the sample weight (mg/mg of tissue). Tension values recorded under 40 V/40 Hz and 80 V/80 Hz stimulation were used to compare the contractility of unlabeled and SPIO-labeled tissue-engineered muscles 4 weeks after injection.

Magnetic resonance imaging

Phantoms were prepared using culture dishes filled with 1.6% agar (Sigma) in PBS. Drill holes (4 mm diameter) were loaded with 35 μL of suspensions with 1.5×10^5 freshly labeled cells in agar. After solidification the drill holes were closed with additional agar.

Mice were subjected to MRI analysis 4 days, 1 week, 2 weeks, and 4 weeks after hMPC transplantation. During the imaging process mice were anesthetized with 1.5% isoflurane.

All measurements were performed in a Bruker 4.7 T Pharmascan 47/16 (Bruker BioSpin MRI GmbH) with a gradient strength of 375 mT/m and a slew rate of 3375 T/m/s equipped with a circular polarized 1H mouse whole body transmit-receive RF coil. After a gradient-echo localizer in three spatial directions, the T2-weighted MR images were acquired using Rapid Acquisition with Relaxation Enhancement sequence (RARE; TE = 15 ms, TR 4500 ms, RARE factor 8, number of averages = 5, slice thickness = 1 mm, FoV 40 × 40 mm, Matrix 384 × 384, and acquisition time 17 min 38 s).

Statistics

Experiments were repeated with hMPCs isolated from at least three human donors. All assays and stainings were performed in triplicate. Data were analyzed by Student's *t*-test or one-way ANOVA with Bonferroni *post hoc* analysis. The results are presented as a mean value ± SD or ± SEM depending on the test. Data with a value $p < 0.05$ were considered as significant.

Results

SPIO labeling of hMPCs

hMPCs labeled for 24 h with SPIOs at different concentrations ranging from 100 to 1600 μg/mL were stained for iron oxides with Prussian blue to assess the labeling efficiency. Directly after labeling, hMPCs displayed an increasingly strong blue staining when exposed to increasing concentrations of SPIOs (Fig. 1a). Notably, nanoparticles concentrated mostly in the perinuclear region of the cytoplasm. One passage after SPIO labeling, the cells still stained positive for iron oxide, although in a more diluted manner (Fig. 1b). Importantly, cell morphology did not change in response to labeling with increasing concentrations of SPIOs. After labeling with SPIOs, hMPCs were also embedded in an agar gel and examined by MRI (Fig. 2). The T2-weighted MR-images showed a decreasing signal with higher concentrations of SPIOs. This inverse monotone behavior could be observed for both, cells imaged directly after labeling (Fig. 2a) and cells imaged one passage after labeling (Fig. 2b), the latter showing, however, a much weaker signal attenuation.

Cytocompatibility of SPIO labeling

Possible toxic effects of the SPIO labeling on hMPCs were assessed by Trypan Blue exclusion assay 24 h after labeling. While cell viability was largely unaffected with nanoparticle concentrations of 100 and 200 μg/mL (Fig. 3a), it was significantly reduced for higher SPIO concentrations, decreasing to 92%, 86%, and 77% for concentrations of 400, 800, and 1600 μg/mL, respectively, showing a linear dependence between SPIO concentration and viability ($r^2 = 0.995$). However, cell growth was not affected by the presence of SPIOs, as growth curves for the different conditions all followed the same S-shaped curve, showing overlapping values up to one passage after labeling (Fig. 3b, c).

Influence of SPIO labeling on the muscle phenotype and differentiation capacity

To confirm the muscle phenotype of the hMPCs, FACS analysis was performed assessing the expression of specific skeletal muscle markers MyoD, MyHC, desmin, and α-actinin (Fig. 4a). Notably, all investigated markers were expressed at similar levels in both the control and the SPIO-labeled cells, with differentiation markers MyHC, desmin, and α-actinin being highly expressed with 95%, 90%, and 97%, respectively, indicating populations of a partly differentiated phenotype. Similarly, immunocytochemical stainings for MyoD, MyHC,

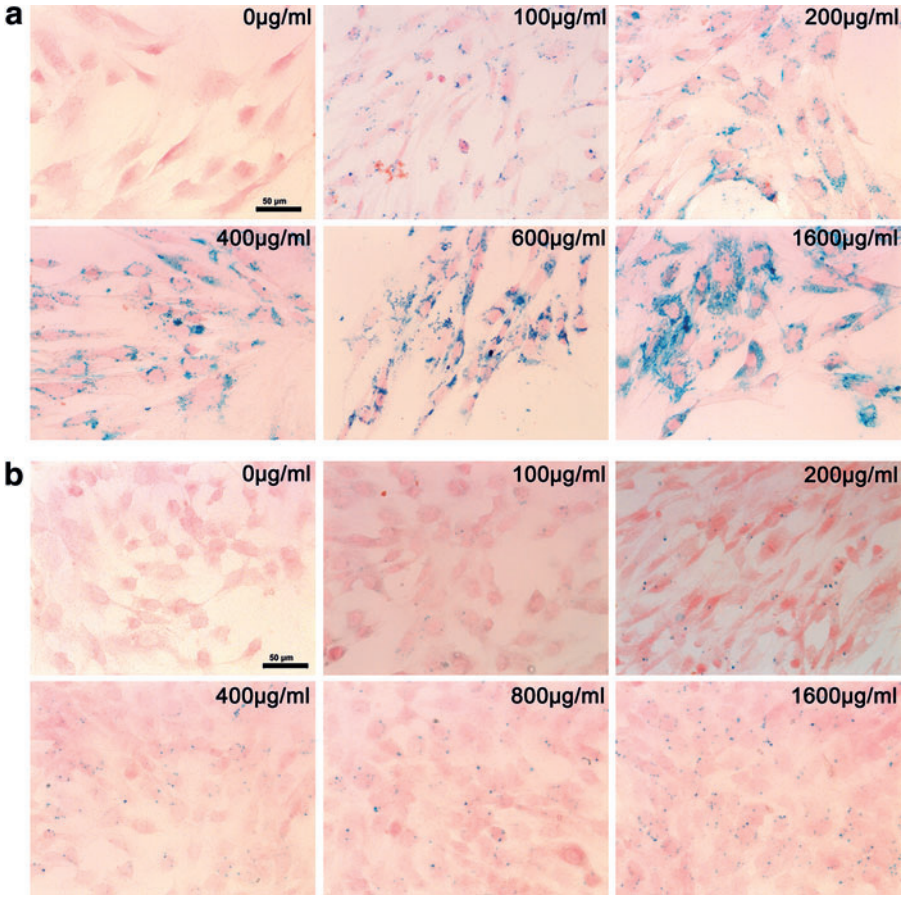

FIG. 1. Superparamagnetic iron oxide (SPIO) uptake by hMPCs. hMPCs were treated with SPIO nanoparticles at concentrations of 0–1600 μg/mL and stained for iron **(a)** directly after SPIO labeling and **(b)** one passage (9 population doublings) after SPIO labeling. Scale bar is 50 μm. hMPCs, human muscle precursor cells. Color images available online at www.liebertpub.com/tec

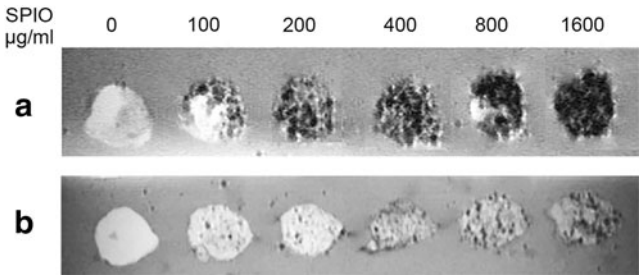

FIG. 2. T2-weighted MR images of SPIO-labeled hMPCs in an agar phantom. 1.5×10^5 hMPCs were treated with SPIO nanoparticle concentrations of 0–1600 µg/mL, embedded in an agar gel and imaged on a 4.7 T magnetic resonance imaging (MRI) system **(a)** directly after SPIO labeling and **(b)** one passage (9 population doublings) after SPIO labeling.

desmin, and α-actinin showed equal expression levels in cells with and without SPIO labeling (Fig. 4b). Furthermore, the fiber formation assay (Supplementary Fig. S1; Supplementary Data are available online at www.liebertpub.com/tec) was used to evaluate the differentiation capacity of hMPCs, showing no significant changes among the investigated concentrations (Fig. 4c, d; 7.4 ± 1.4 nuclei per fiber formed; 22.7% ± 4.3% differentiation ratio).

Tracking of hMPCs in vivo

Evaluating the ability to track hMPCs in an *in vivo* environment, either labeled (400 µg/mL) or nonlabeled hMPCs were mixed with a collagen solution, injected subcutaneously in the backsides of nude mice, and imaged by MRI (Fig. 5). Over the period of 4 weeks, T2-weighted MRI images clearly showed the position of the injected hMPCs as a protuberance in the subcutaneous area. While the control cells displayed a bright signal, the labeled cells appeared dark due to the signal loss caused by the presence of SPIOs. Over time, the volume of the injected hMPCs decreased, showing a reduction in sample weight from day 14 to 28 of 16.7% (data not shown).

Evaluation of in vivo *muscle formation by histological analysis*

To assess the myogenic *in vivo* differentiation of the injected hMPCs, the newly formed tissue was evaluated by histological analysis (Fig. 6). Macroscopically, the tissue-engineered muscle was a distinct object in the subcutaneous space of nude mice, remaining at the site of injection throughout the experiment. H&E staining and immunohistochemical stainings of both labeled and nonlabeled hMPCs showed distinct myofibers that strongly expressed skeletal muscle marker proteins desmin, MyHC, and α-actinin (Fig. 6a). The sections also showed longitudinally or transversely cut muscle fibers with sarcomeric striations and centrally and peripherally localized nuclei. PKH67 labeling of the hMPCs furthermore demonstrated that the newly formed muscle tissue was formed by human cells only (Supplementary Fig. S2).

Simultaneously, tissue sections were stained by Prussian blue to facilitate iron detection (Fig. 6b). When staining tissue-engineered fibers originating from nonlabeled cells, no iron was detected. In tissue sections from mice injected with 400 µg/mL SPIO-labeled MPCs, large accumulation of iron oxide could be detected over the course of 4 weeks. Iron particles were present within the newly formed muscle fibers after 4 weeks postinjection, but could also be observed localized to single cells (Fig. 6c). In some regions of the engineering muscle tissue, staining for mouse macrophages using an F4/80 antibody revealed co-localization of the iron oxide nanoparticles with macrophages (Fig. 6d).

Functionality of newly formed muscle tissue

Functionality of the tissue-engineered muscle was assessed via myography. The tissues displayed distinct muscle contractions after electrical stimulation of 40 V/40 Hz and 80 V/80 Hz (Fig. 7). Contractile forces of muscle formed by SPIO-labeled MPCs were comparable to the ones originating from MPCs without SPIO labeling at 40 V/40 Hz and displayed a statistically not significant difference at 80 V/80 Hz.

Discussion

Monitoring the fate, distribution, and engraftment of the stem cells in the host is a major concern in cell therapy concepts. Therefore, reliable and noninvasive tracking of the cells *in vivo* is of great interest before translation of such approaches to clinical routine use. There are many imaging techniques and labeling strategies available for noninvasive live cell tracking, each possessing unique advantages but also distinct disadvantages.[36] Among those approaches, monitoring of SPIO-labeled cells *in vivo* by MRI has shown

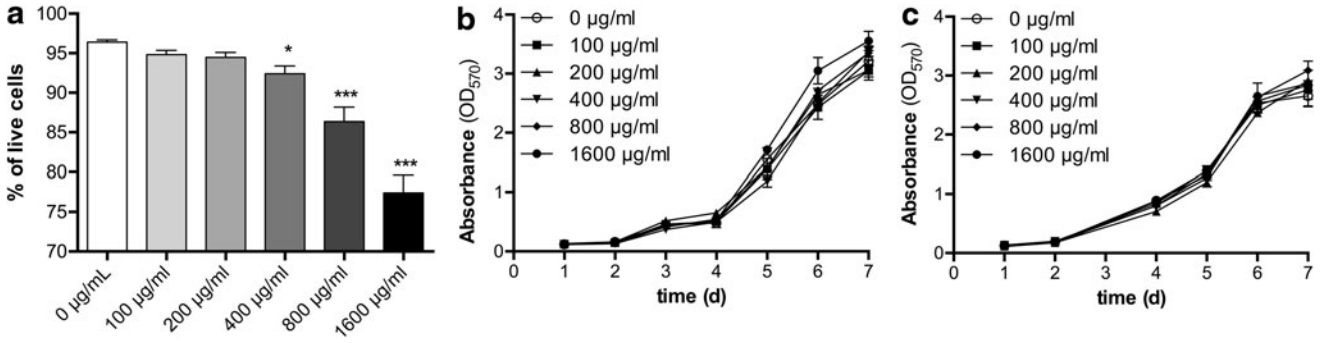

FIG. 3. Assessment of cell viability and cell growth after SPIO labeling. hMPCs were treated with SPIO nanoparticles at concentrations of 0–1600 µg/mL. **(a)** Viability of labeled hMPCs was assessed via Trypan Blue exclusion assay 24 h after SPIO treatment (one-way ANOVA, $*p < 0.05$ $***p < 0.001$ compared to control). Growth curves of labeled hMPCs were obtained via MTT assay **(b)** 24 h after SPIO labeling and **(c)** one passage (9 population doublings) after SPIO labeling.

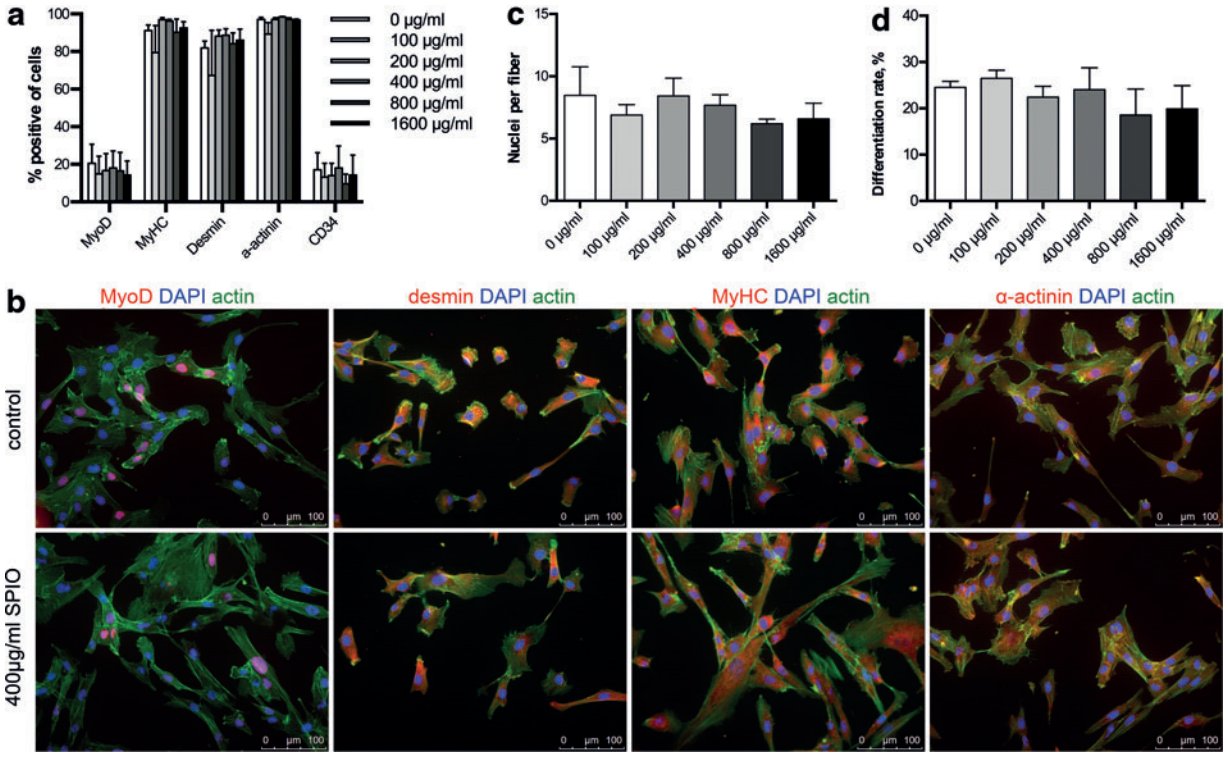

FIG. 4. Analysis of muscle-specific protein expression and myogenic differentiation capacity of hMPCs after SPIO labeling. hMPCs were treated with SPIO nanoparticles at concentrations of 0–1600 µg/mL and evaluated for expression of muscle-specific proteins one passage (9 population doublings) after SPIO labeling via **(a)** FACS analysis and **(b)** immunostaining (only unlabeled and 400 µg/mL SPIO labeled cells are shown). Differentiation capacity of labeled MPCs one passage after SPIO labeling was evaluated in terms of **(c)** myotube size (nuclei per fiber) and **(d)** differentiation ratio (percent of all nuclei fused into fibers). Scale bar is 100 µm. Color images available online at www.liebertpub.com/tec

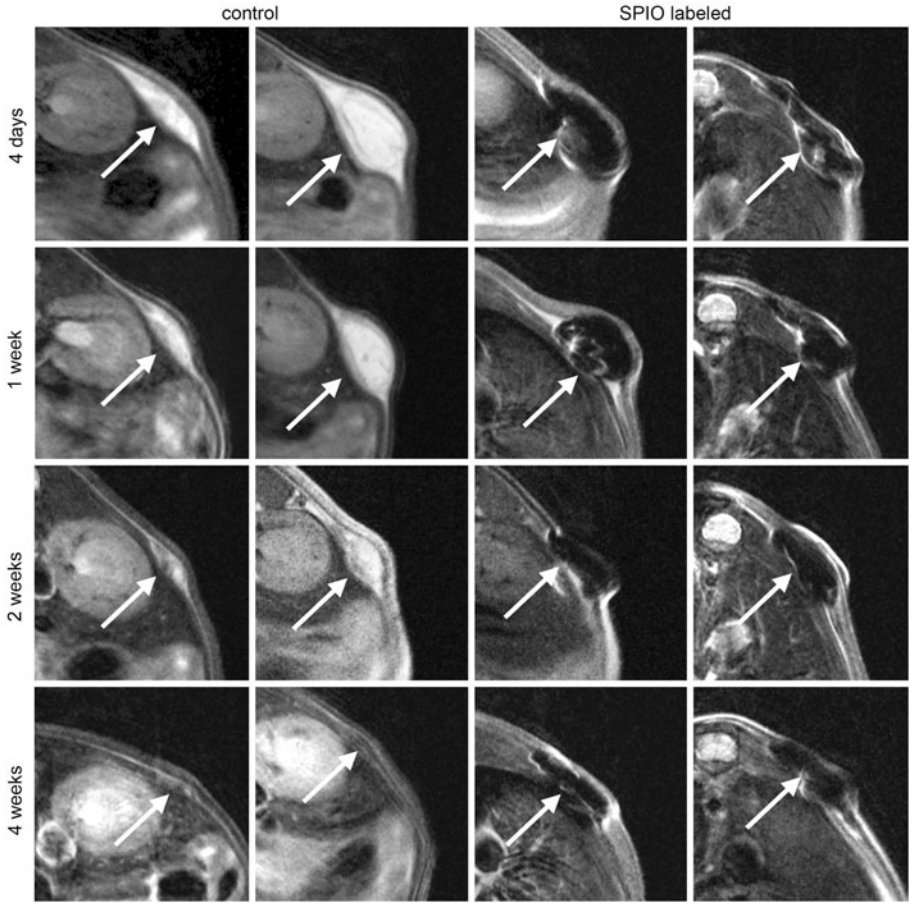

FIG. 5. Tracking of transplanted hMPCs by MRI. Unlabeled (control) and 400 µg/mL labeled hMPCs were subcutaneously injected in the back of nude mice before scanning by MRI 4 days, 1 week, 2 weeks, and 4 weeks after injection. The area of interest in representative T2-weighted MRI images is shown and injected cells are marked with an arrow. Two representative mice are shown for injections with both control cells and SPIO-labeled hMPCs.

great promise,[20] but its safety and efficacy has to be evaluated for each cell type and SPIO independently.

While cells are generally capable of absorbing iron oxide nanoparticles by endocytosis, nonphagocytic or slow dividing cells usually require the use of a transfection reagent to enhance the uptake,[30,31,34,37] which by itself can have adverse effects on cells.[38] Furthermore, the use of such agents may complicate translation into clinics, as substances like poly-L-lysine lack FDA-approval. In this study, hMPCs incorporated the SPIO nanoparticles in a concentration-dependent manner, showing a homogeneous distribution of the particles even without the addition of a transfection reagent (Fig. 1). This is in good agreement with an early work, which demonstrated that porcine skeletal muscle-derived cells were efficiently labeled with SPIOs alone.[39] Similarly, human MSCs (hMSCs) could also be labeled with SPIOs alone, however, the efficiency was lower when compared with novel citrate-coated SPIOs.[40] As the internalization step is nonspecific and happens via endocytosis, the absorption rate is influenced not only by the size[41,42] but also by the coating[40,43–45] of the SPIOs. Nanoparticle uptake appears to be furthermore dependent on the exact cell type, as in a murine model, muscle-derived stem cells displayed a poor labeling efficiency with SPIOs alone and necessitated the application of a transfection agent.[46] Interestingly, showing almost complete loss of SPIOs by MSCs between 7 and 22 days *in vitro*, not only SPIO uptake, but also intracellular retention of the nanoparticles was demonstrated to be cell- and nanoparticle-type dependent.[47] In good agreement, culture expansion of hMPCS for one passage ($\sim$7 days) similarly displayed a strong reduction in intracellular iron staining (Fig. 1), suggesting that the loss of SPIOs occurs due to the rapid proliferation of the cells *in vitro*.

Coated SPIO nanoparticles are generally considered to be relatively nontoxic[48] and while a high SPIO uptake efficiency

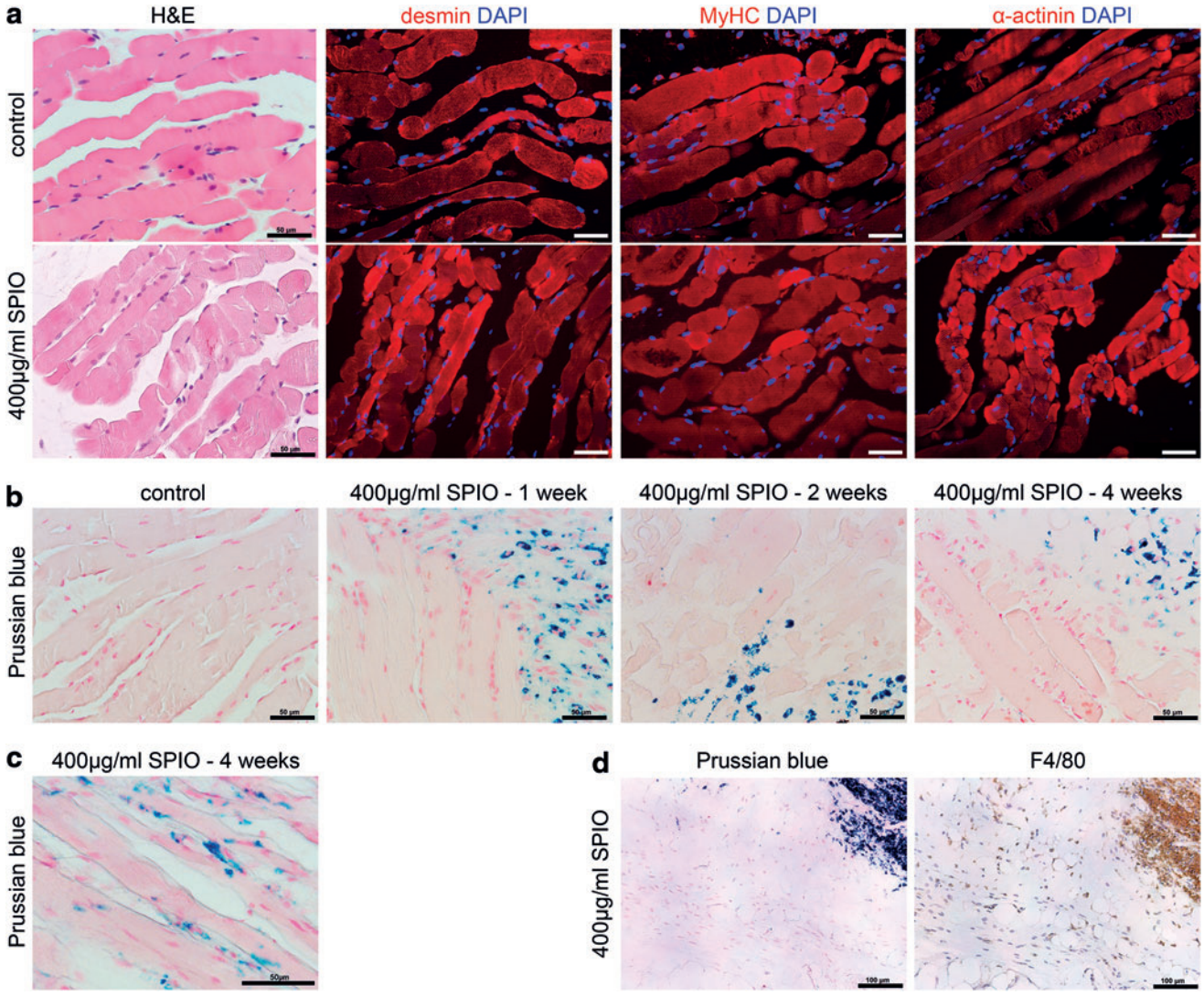

FIG. 6. Histological analysis of the newly formed muscle tissues. After myogenic *in vivo* differentiation, tissues formed by unlabeled (control) and 400 µg/mL labeled hMPCs were harvested and evaluated by **(a)** H&E staining and immunostaining for muscle markers desmin, myosin heavy chain (MyHC), and α-actinin 4 weeks after MPC injection; scale bar is 50 µm and **(b)** Prussian blue staining for iron after 1, 2, and 4 weeks after injection, with a higher magnification shown in **(c)** Scale bar is 50 µm. **(d)** Uptake of SPIO nanoparticles by macrophages was evaluated 4 weeks after injection via co-staining with Prussian blue and marker F4/80 for mouse macrophages. Scale bar is 100 µm. H&E, hematoxylin and eosin. Color images available online at www.liebertpub.com/tec

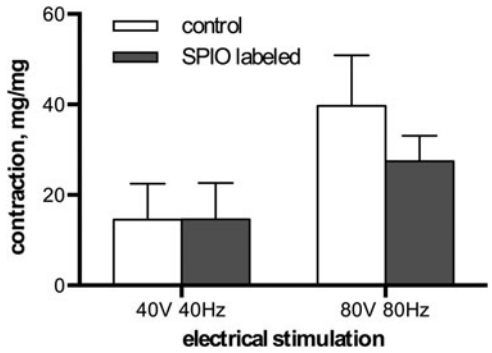

FIG. 7. Assessment of tissue contractility via myography. After 4 weeks of myogenic *in vivo* differentiation, tissues formed by unlabeled (control) and 400 μg/mL labeled hMPCs were harvested and contractility was assessed in response to 40 V/40 Hz and 80 V/80 Hz electrical stimulation. Contractions of three muscle tissues normalized to their weight (mg/mg) were used for comparison.

is desirable from an imaging standpoint, high nanoparticle loads can have negative effects on cell viability and differentiation.[23–25,27–30,40] Data regarding possible negative effects of SPIO labeling are, however, difficult to compare, and while the majority of studies did not show detrimental effects on various cell types,[20] an inhibitory effect of SPIO labeling on chondrogenic but not adipogenic or osteogenic differentiation of hMSCs at a concentration of 500 μg/mL has been shown recently.[40] Being in good agreement with the majority of studies, the results in this work displayed no negative effect on cell viability at concentrations up to 200 μg/mL with only a minor decrease at 400 μg/mL. At concentrations of 800 and 1600 μg/mL however, viability decreased significantly (Fig. 3a). Interestingly, there were no changes in the proliferation rate (Fig. 3b, c), expression of skeletal markers, or differentiation capacity (Fig. 4) of hMPCs irrespective of the SPIO concentration, suggesting that myogenic differentiation is a more robust process compared with chondrogenic differentiation of hMSCs.

Regarding the optimal SPIO concentration for MRI cell tracking, previous work has shown a correlation between the applied nanoparticle concentration and loss of MRI signal intensity.[40] This is in good agreement with the results observed in this study, showing a concentration-dependent MRI signal loss, which was very high directly after labeling of hMPCs, and while much weaker, still well detectable after one passage of proliferation, which corresponds to 9 population doublings (Fig. 2). About 400 μg/mL was found to be best compromise between a high nanoparticle load, a high signal alteration in MR images, and a minimal negative effect on cell viability and was thus implemented for all subsequent experiments. When injecting the SPIO-labeled hMPCs into the subcutaneous space of nude mice, the cells were visible as a hypointense entity in the MR images over a period of 4 weeks (Fig. 5). Similar time frames have been reported previously when tracking SPIO-labeled cells *in vivo*.[46,49] The observed discrepancy between the rapid loss of labeling *in vitro* and the extended signal retention *in vivo* can possibly be explained twofold. On the one hand, the cells *in vitro* were kept in a proliferative state undergoing several rounds of cell division, whereas *in vivo*, the cells only fused once to form mature muscle fibers. On the other hand, SPIOs lost by the cells *in vitro* were removed upon changing the medium but were taken up by macrophages in the vicinity of the hMPCs *in vivo* (Fig. 6), thereby continuing to contribute to the negative MRI-signal, which is a problem inherent to SPIO labeling cells. Noteworthy, unlabeled MPCs were also visible in the MRI as a well-defined hyperintense area for at least 2 weeks, potentially reflecting fluid from the injection, a local inflammatory reaction or a combination of the two, but injections were hardly detectable thereafter. Based on the MR images with labeled hMPCs and measurements of sample weights after 2 and 4 weeks *in vivo*, the injection volume greatly decreased over the course of 4 weeks, which likely occurs due to the fusion of cells into myofibers and the concomitant remodeling of the collagen carrier. While the subcutaneous injections of labeled cells can be detected in T2-weighted images over the course of up to 4 weeks despite this shrinkage, localizing unlabeled cells may not be possible when applied as an intramuscular injection.

In stem cell therapy approaches, the fate of the injected cells *in vivo* is a major concern and even though autologous adult stem or progenitor cells are generally considered to be safe, the *in vitro* expansion and manipulation procedures may adversely affect the therapeutic quality of the cells.[12] While whole myofiber implants have been suggested as a superior alternative to culture expanded muscle progenitor cells,[50] immunohistofluorescence stainings demonstrated that both the labeled and unlabeled cells formed muscle fibers, which strongly expressed specific markers of skeletal muscles (Fig. 6). Moreover, functionality of the newly formed muscle tissue could be demonstrated by myography (Fig. 7), confirming that hMPCs isolated from patient biopsies retain their capacity to form contractile muscle tissue after *in vitro* culture expansion and SPIO labeling. Using the identical protocol for hMPC isolation and *in vitro* culture expansion, it was previously demonstrated that such cells were able to restore a damaged sphincter muscle in dogs for up to 6 months.[14] Similar results were also obtained in rats using allogenic MPCs.[51]

A further aspect when injecting labeled cells *in vivo* is the localization of SPIO in the engineered tissue. SPIO nanoparticles cleared from the cells over time through exocytosis, when cells undergo cell division or upon cell death can be taken up by the monocyte/macrophage system[52,53] and the potential transfer/uptake of SPIO nanoparticles by macrophages from labeled hMSCs has been shown previously.[54] In this study, tissue sections of bioengineered muscle tissue revealed that nanoparticles remained inside the newly formed muscle fibers but could also be detected localized to tissue macrophages (Fig. 6). While this suggests that nanoparticles were cleared to some extent from the hMPCs during the fusion process of myofiber formation, the injected hMPCs were not engulfed by macrophages but instead formed functional muscle tissue. Importantly, the sensitivity of the MRI can be adjusted by altering the sequence parameters (i.e., shorter/longer echo time TE), and the amount of SPIO nanoparticles incorporated in muscle fibers could thus still enable long-term cell tracking upon macrophage clearance from the site of injection.

Unfortunately, Endorem has been taken from the market for commercial reasons and also Resovist is no longer commercially available. However, with cell therapy being a research area of great interest and potential, it is likely only a matter of time before more contrast agents will be available or

before production of discontinued agents such as Endorem will be resumed. For example, Ferumoxytol (Feraheme®), an ultrasmall SPIO that has recently been approved by the FDA for iron supplementation therapy, efficiently labels hMSCs when used off-label.[55]

Conclusion

The herein presented data clearly demonstrate that primary hMPCs can be labeled with an FDA approved SPIO without the use of an additional transfection agent and that the labeled cells retain the expression of characteristic markers of skeletal muscles and form functional tissue engineered skeletal muscle *in vivo*. Furthermore, the location of the stem cell injection can be visualized by MRI *in vivo* up to 1 month. Such a monitoring strategy is essential to ensure safety and efficacy of future cell therapies for muscle regeneration in patients affected by SUI and other applications in regenerative medicine.

Acknowledgments

We would like to thank Damina Balmer for her help with preparing the article, Pia Fuchs for her assistance with histology, and Udo Ungethüm and Josiane Njiwa for their assistance with MR imaging. We acknowledge the financial support by the Swiss National Fund (SNF; grant number 32323B_144935) and the Klinischer Forschungsschwerpunkt ''Molecular Imaging Network Zurich'' (KFSP MINZ).

Disclosure Statement

No competing financial interests exist.

References

1. Brown, J.S., Nyberg, L.M., Kusek, J.W., Burgio, K.L., Diokno, A.C., Foldspang, A., *et al.* Proceedings of the National Institute of Diabetes and Digestive and Kidney Diseases International Symposium on Epidemiologic Issues in Urinary Incontinence in Women. Am J Obstet Gynecol **188,** 77, 2003.
2. Wilson, L., Brown, J.S., Shin, G.P., Luc, K.O., and Subak, L.L. Annual direct cost of urinary incontinence. Obstet Gynecol **98,** 398, 2001.
3. Holroyd-Leduc, J.M., and Straus, S.E. Management of urinary incontinence in women: scientific review. JAMA **291,** 986, 2004.
4. Nikolavasky, D., Stangel-Wojcikiewicz, K., Stec, M., and Chancellor, M.B. Stem cell therapy: a future treatment of stress urinary incontinence. Semin Reprod Med **29,** 61, 2011.
5. Rovner, E.S., and Wein, A.J. Treatment options for stress urinary incontinence. Rev Urol **6 Suppl 3,** S29, 2004.
6. Atala, A. Advances in tissue and organ replacement. Curr Stem Cell Res Ther **3,** 21, 2008.
7. Bajada, S., Mazakova, I., Richardson, J.B., and Ashammakhi, N. Updates on stem cells and their applications in regenerative medicine. J Tissue Eng Regen Med **2,** 169, 2008.
8. Ptaszek, L.M., Mansour, M., Ruskin, J.N., and Chien, K.R. Towards regenerative therapy for cardiac disease. Lancet **379,** 933, 2012.
9. Lindvall, O., and Kokaia, Z. Stem cells in human neurodegenerative disorders—time for clinical translation? J Clin Invest **120,** 29, 2010.
10. Bernardi, S., Severini, G.M., Zauli, G., and Secchiero, P. Cell-based therapies for diabetic complications. Exp Diabetes Res **2012,** 872504, 2012.
11. Negroni, E., Vallese, D., Vilquin, J.T., Butler-Browne, G., Mouly, V., and Trollet, C. Current advances in cell therapy strategies for muscular dystrophies. Expert Opin Biol Ther **11,** 157, 2011.
12. Gras, S., and Lose, G. The clinical relevance of cell-based therapy for the treatment of stress urinary incontinence. Acta Obstet Gynecol Scand **90,** 815, 2011.
13. Wang, H.J., Chuang, Y.C., and Chancellor, M.B. Development of cellular therapy for the treatment of stress urinary incontinence. Int Urogynecol J **22,** 1075, 2011.
14. Eberli, D., Aboushwareb, T., Soker, S., Yoo, J.J., and Atala, A. Muscle precursor cells for the restoration of irreversibly damaged sphincter function. Cell Transplant **21,** 2089, 2012.
15. Kircher, M.F., Gambhir, S.S., and Grimm, J. Noninvasive cell-tracking methods. Nat Rev Clin Oncol **8,** 677, 2011.
16. Manley, N.C., and Steinberg, G.K. Tracking stem cells for cellular therapy in stroke. Curr Pharm Des **18,** 3685, 2012.
17. Anderson, S.A., Glod, J., Arbab, A.S., Noel, M., Ashari, P., Fine, H.A., *et al.* Noninvasive MR imaging of magnetically labeled stem cells to directly identify neovasculature in a glioma model. Blood **105,** 420, 2005.
18. Iwanami, A., Kaneko, S., Nakamura, M., Kanemura, Y., Mori, H., Kobayashi, S., *et al.* Transplantation of human neural stem cells for spinal cord injury in primates. J Neurosci Res **80,** 182, 2005.
19. Runge, V.M. Current technological advances in magnetic resonance with critical impact for clinical diagnosis and therapy. Invest Radiol **48,** 869, 2013.
20. Cromer Berman, S.M., Walczak, P., and Bulte, J.W. Tracking stem cells using magnetic nanoparticles. Wiley Interdiscip Rev Nanomed Nanobiotechnol **3,** 343, 2011.
21. Wang, Y.X. Superparamagnetic iron oxide based MRI contrast agents: current status of clinical application. Quant Imaging Med Surg **1,** 35, 2011.
22. Niemeyer, M., Oostendorp, R.A., Kremer, M., Hippauf, S., Jacobs, V.R., Baurecht, H., *et al.* Non-invasive tracking of human haemopoietic CD34(+) stem cells *in vivo* in immunodeficient mice by using magnetic resonance imaging. Eur Radiol **20,** 2184, 2010.
23. Rice, H.E., Hsu, E.W., Sheng, H., Evenson, D.A., Freemerman, A.J., Safford, K.M., *et al.* Superparamagnetic iron oxide labeling and transplantation of adipose-derived stem cells in middle cerebral artery occlusion-injured mice. AJR Am J Roentgenol **188,** 1101, 2007.
24. Song, Y.S., and Ku, J.H. Monitoring transplanted human mesenchymal stem cells in rat and rabbit bladders using molecular magnetic resonance imaging. Neurourol Urodyn **26,** 584, 2007.
25. Sun, J.H., Zhang, Y.L., Nie, C.H., Qian, S.P., Yu, X.B., Xie, H.Y., *et al. In vitro* labeling of endothelial progenitor cells isolated from peripheral blood with superparamagnetic iron oxide nanoparticles. Mol Med Rep **6,** 282, 2012.
26. Watson, D.J., Walton, R.M., Magnitsky, S.G., Bulte, J.W., Poptani, H., and Wolfe, J.H. Structure-specific patterns of neural stem cell engraftment after transplantation in the adult mouse brain. Hum Gene Ther **17,** 693, 2006.
27. Chen, Y.C., Hsiao, J.K., Liu, H.M., Lai, I.Y., Yao, M., Hsu, S.C., *et al.* The inhibitory effect of superparamagnetic iron oxide nanoparticle (Ferucarbotran) on osteogenic differentiation and its signaling mechanism in human mesenchymal stem cells. Toxicol Appl Pharmacol **245,** 272, 2010.
28. Kostura, L., Kraitchman, D.L., Mackay, A.M., Pittenger, M.F., and Bulte, J.W. Feridex labeling of mesenchymal

stem cells inhibits chondrogenesis but not adipogenesis or osteogenesis. NMR Biomed **17,** 513, 2004.
29. Schafer, R., Kehlbach, R., Muller, M., Bantleon, R., Kluba, T., Ayturan, M., *et al.* Labeling of human mesenchymal stromal cells with superparamagnetic iron oxide leads to a decrease in migration capacity and colony formation ability. Cytotherapy **11,** 68, 2009.
30. van Buul, G.M., Kotek, G., Wielopolski, P.A., Farrell, E., Bos, P.K., Weinans, H., *et al.* Clinically translatable cell tracking and quantification by MRI in cartilage repair using superparamagnetic iron oxides. PLoS One **6,** e17001, 2011.
31. Arbab, A.S., Bashaw, L.A., Miller, B.R., Jordan, E.K., Bulte, J.W., and Frank, J.A. Intracytoplasmic tagging of cells with ferumoxides and transfection agent for cellular magnetic resonance imaging after cell transplantation: methods and techniques. Transplantation **76,** 1123, 2003.
32. Boulland, J.L., Leung, D.S., Thuen, M., Vik-Mo, E., Joel, M., Perreault, M.C., *et al.* Evaluation of intracellular labeling with micron-sized particles of iron oxide (MPIOs) as a general tool for *in vitro* and *in vivo* tracking of human stem and progenitor cells. Cell Transplant **21,** 1743, 2012.
33. van Buul, G.M., Farrell, E., Kops, N., van Tiel, S.T., Bos, P.K., Weinans, H., *et al.* Ferumoxides-protamine sulfate is more effective than ferucarbotran for cell labeling: implications for clinically applicable cell tracking using MRI. Contrast Media Mol Imaging **4,** 230, 2009.
34. Zhu, W., Li, X., Tang, Z., Zhu, S., Qi, J., Wei, L., *et al.* Superparamagnetic iron oxide labeling of neural stem cells and 4.7T MRI tracking *in vivo* and *in vitro*. J Huazhong Univ Sci Technolog Med Sci **27,** 107, 2007.
35. Eberli, D., Soker, S., Atala, A., and Yoo, J.J. Optimization of human skeletal muscle precursor cell culture and myofiber formation *in vitro*. Methods **47,** 98, 2009.
36. Frangioni, J.V., and Hajjar, R.J. *In vivo* tracking of stem cells for clinical trials in cardiovascular disease. Circulation **110,** 3378, 2004.
37. Arbab, A.S., Yocum, G.T., Kalish, H., Jordan, E.K., Anderson, S.A., Khakoo, A.Y., *et al.* Efficient magnetic cell labeling with protamine sulfate complexed to ferumoxides for cellular MRI. Blood **104,** 1217, 2004.
38. Arbab, A.S., Yocum, G.T., Wilson, L.B., Parwana, A, Jordan, E.K., Kalish, H., *et al.* Comparison of transfection agents in forming complexes with ferumoxides, cell labeling efficiency, and cellular viability. Mol Imaging **3,** 24, 2004.
39. Garot, J., Unterseeh, T., Teiger, E., Champagne, S., Chazaud, B., Gherardi, R., *et al.* Magnetic resonance imaging of targeted catheter-based implantation of myogenic precursor cells into infarcted left ventricular myocardium. J Am Coll Cardiol **41,** 1841, 2003.
40. Andreas, K., Georgieva, R., Ladwig, M., Mueller, S., Notter, M., Sittinger, M., *et al.* Highly efficient magnetic stem cell labeling with citrate-coated superparamagnetic iron oxide nanoparticles for MRI tracking. Biomaterials **33,** 4515, 2012.
41. Oude Engberink, R.D., van der Pol, S.M., Dopp, E.A., de Vries, H.E., and Blezer, E.L. Comparison of SPIO and USPIO for *in vitro* labeling of human monocytes: MR detection and cell function. Radiology **243,** 467, 2007.
42. Thorek, D.L., and Tsourkas, A. Size, charge and concentration dependent uptake of iron oxide particles by nonphagocytic cells. Biomaterials **29,** 3583, 2008.
43. Ittrich, H., Lange, C., Dahnke, H., Zander, A.R., Adam, G., and Nolte-Ernsting, C. [Labeling of mesenchymal stem cells with different superparamagnetic particles of iron oxide and detectability with MRI at 3T]. Rofo **177,** 1151, 2005.
44. Wang, H.H., Wang, Y.X., Leung, K.C., Au, D.W., Xuan, S., Chak, C.P., *et al.* Durable mesenchymal stem cell labelling by using polyhedral superparamagnetic iron oxide nanoparticles. Chemistry **15,** 12417, 2009.
45. Zhu, X.M., Wang, Y.X., Leung, K.C., Lee, S.F., Zhao, F., Wang, D.W., *et al.* Enhanced cellular uptake of aminosilane-coated superparamagnetic iron oxide nanoparticles in mammalian cell lines. Int J Nanomed **7,** 953, 2012.
46. Cahill, K.S., Gaidosh, G., Huard, J., Silver, X., Byrne, B.J., and Walter, G.A. Noninvasive monitoring and tracking of muscle stem cell transplants. Transplantation **78,** 1626, 2004.
47. Julke, H., Veit, C., Ribitsch, I., Brehm, W., Ludewig, E., and Delling, U. Comparative labelling of equine and ovine multipotent stromal cells with superparamagnetic iron oxide particles for magnetic resonance imaging *in vitro*. Cell Transplant 2013 [Epub ahead of print]; PMID: 24330785.
48. Lewinski, N., Colvin, V., and Drezek, R. Cytotoxicity of nanoparticles. Small **4,** 26, 2008.
49. Neri, M., Maderna, C., Cavazzin, C., Deidda-Vigoriti, V., Politi, L.S., Scotti, G., *et al.* Efficient *in vitro* labeling of human neural precursor cells with superparamagnetic iron oxide particles: relevance for *in vivo* cell tracking. Stem Cells **26,** 505, 2008.
50. Riviere, C., Lecoeur, C., Wilhelm, C., Pechoux, C., Combrisson, H., Yiou, R., *et al.* The MRI assessment of intraurethrally—delivered muscle precursor cells using anionic magnetic nanoparticles. Biomaterials **30,** 6920, 2009.
51. Cannon, T.W., Lee, J.Y., Somogyi, G., Pruchnic, R., Smith, C.P., Huard, J., *et al.* Improved sphincter contractility after allogenic muscle-derived progenitor cell injection into the denervated rat urethra. Urology **62,** 958, 2003.
52. Longmire, M., Choyke, P.L., and Kobayashi, H. Clearance properties of nano-sized particles and molecules as imaging agents: considerations and caveats. Nanomedicine (London, England) **3,** 703, 2008.
53. Luciani, N., Wilhelm, C., and Gazeau, F. The role of cell-released microvesicles in the intercellular transfer of magnetic nanoparticles in the monocyte/macrophage system. Biomaterials **31,** 7061, 2010.
54. Pawelczyk, E., Jordan, E.K., Balakumaran, A., Chaudhry, A., Gormley, N., Smith, M., *et al. In vivo* transfer of intracellular labels from locally implanted bone marrow stromal cells to resident tissue macrophages. PLoS One **4,** e6712, 2009.
55. Castaneda, R.T., Khurana, A., Khan, R., and Daldrup-Link, H.E. Labeling stem cells with ferumoxytol, an FDA-approved iron oxide nanoparticle. J Vis Exp **57,** e3482, 2011.

Address correspondence to:
Daniel Eberli, MD, PhD
Division of Urology
University Hospital Zurich
Frauenklinikstr. 10
Zurich CH-8091
Switzerland

E-mail: daniel.eberli@usz.ch

Received: February 2, 2014
Accepted: June 23, 2014
Online Publication Date: August 1, 2014